

## Accepted Manuscript

Interaction of dequalinium chloride with phosphatidylcholine bilayers: a biophysical study with consequences on the development of lipid-based mitochondrial nanomedicines

Félix Sauvage, François-Xavier Legrand, Michel Roux, Ivan Rajkovic, Thomas M. Weiss, Zoltán Varga, Luc Augis, Guillaume Nugue, Jean-Claude Debouzy, Juliette Vergnaud-Gauduchon, Gillian Barratt

PII: S0021-9797(18)31373-0  
DOI: <https://doi.org/10.1016/j.jcis.2018.11.059>  
Reference: YJCIS 24324

To appear in: *Journal of Colloid and Interface Science*

Received Date: 13 July 2018  
Revised Date: 13 November 2018  
Accepted Date: 14 November 2018

Please cite this article as: F. Sauvage, F-X. Legrand, M. Roux, I. Rajkovic, T.M. Weiss, Z. Varga, L. Augis, G. Nugue, J-C. Debouzy, J. Vergnaud-Gauduchon, G. Barratt, Interaction of dequalinium chloride with phosphatidylcholine bilayers: a biophysical study with consequences on the development of lipid-based mitochondrial nanomedicines, *Journal of Colloid and Interface Science* (2018), doi: <https://doi.org/10.1016/j.jcis.2018.11.059>

This is a PDF file of an unedited manuscript that has been accepted for publication. As a service to our customers we are providing this early version of the manuscript. The manuscript will undergo copyediting, typesetting, and review of the resulting proof before it is published in its final form. Please note that during the production process errors may be discovered which could affect the content, and all legal disclaimers that apply to the journal pertain.



**Interaction of dequalinium chloride with phosphatidylcholine bilayers: a biophysical study with consequences on the development of lipid-based mitochondrial nanomedicines**

Félix Sauvage<sup>a,1</sup>, François-Xavier Legrand<sup>a,1,\*</sup>, Michel Roux<sup>b</sup>, Ivan Rajkovic<sup>c</sup>, Thomas M. Weiss<sup>c</sup>, Zoltán Varga<sup>d</sup>, Luc Augis<sup>a</sup>, Guillaume Nugue<sup>e</sup>, Jean-Claude Debouzy<sup>e</sup>, Juliette Vergnaud-Gauduchon<sup>a</sup> and Gillian Barratt<sup>a,\*</sup>

<sup>a</sup> Institut Galien Paris-Sud, Univ. Paris-Sud, CNRS, Université Paris-Saclay, 92290 Châtenay-Malabry, France.

<sup>b</sup> Institut de Biologie Intégrative de la Cellule, CNRS, Univ. Paris-Sud, CEA, Université Paris-Saclay, 91190, Gif-Sur-Yvette, France.

<sup>c</sup> Stanford Synchrotron Radiation Lightsource, SLAC National Accelerator Center, Menlo Park, California 94025, United States of America.

<sup>d</sup> Biological Nanochemistry Research Group, Institute of Materials and Environmental Chemistry, Research Centre for Natural Sciences, Hungarian Academy of Sciences, Magyar tudósok körútja 2, 1117 Budapest, Hungary.

<sup>e</sup> Institut de Recherche Biomédicale des Armées, Service de Santé des Armées, 91220, Brétigny-sur-Orge, France.

\* Corresponding authors: e-mail addresses: francois-xavier.legrand@u-psud.fr (F.-X. Legrand), gillian.barratt@u-psud.fr (G. Barratt)

<sup>1</sup> These authors contributed equally to this work.

**Abstract**

Dequalinium (DQ) has been proposed as a mitochondrial targeting ligand for nanomedicines, including liposomes, given the implication of these organelles in many diseases. This original study focuses on the interactions of DQ with phosphatidylcholine bilayers during the formation of liposomes. Firstly, PEGylated liposomes suitable for drug delivery were studied and were found to be more stable when made in water than in phosphate-buffered saline, emphasizing the role of electrostatic interactions between positive charges on DQ and the polar head groups of the lipids. To gain more information, differential scanning calorimetry, small- and wide-angle X-ray scattering and diffraction,  $^{31}\text{P}$  and  $^2\text{H}$  NMR spectroscopy and freeze-fracture electron microscopy were performed on dimyristoylphosphatidylcholine (DMPC) model membranes in the presence of DQ. This molecule was shown to be located at the level of polar head groups and to induce electrostatic repulsions between adjacent lipid bilayers leading to membrane budding in water. These findings indicate that DQ is not completely inert towards lipid membranes and therefore is not an ideal candidate for encapsulation in liposomes. Overall, our work stresses the necessity for thorough physico-chemical characterization to better understand the mechanisms underlying the development of nanomedicines.

*Keywords: liposomes; mitochondria; bilayers; calorimetry; X-ray scattering; NMR spectroscopy; drug delivery; dequalinium.*

## 1 Introduction

Delivering drugs to mitochondria could be a useful strategy in cancer therapy because the mitochondrion has been shown to have an important role in metabolism, redox status and apoptosis. However, knowledge of mitochondria-related pathologies is still very limited, highlighting the need for further studies. Often, these disorders have dramatic consequences, because a single mutation in mitochondrial DNA can generate many different diseases.<sup>1</sup> Over the last two decades, several strategies to specifically target mitochondria have been developed, including the use of functionalized nanoparticles and the development of prodrugs with targeting moieties covalently attached. Among the molecules that can be used to achieve targeting, many are positively charged and lipophilic, able to accumulate within mitochondria due to a greater potential difference across the mitochondrial membrane compared with the plasma membrane; examples are rhodamine 123 chloride (R123), stearyltriphenylphosphonium bromide (STPP) and dequalinium chloride (DQ). In particular, DQ is a symmetrical molecule with two charged regions separated by an alkyl chain ( $n = 10$ ) and is related to bolaamphiphiles (Figure 1).

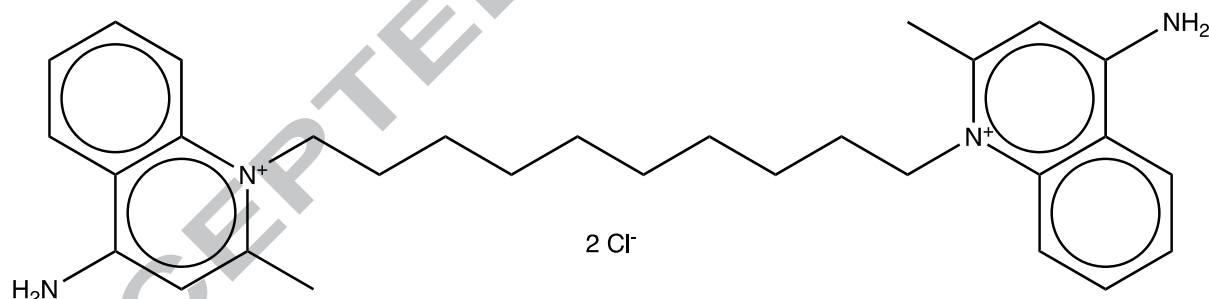


**Figure 1 Chemical representation of the cationic bolaamphiphile dequalinium.**

DQ was first used as a topical antimicrobial agent in the 1950's,<sup>2</sup> showing a broad fungicidal and bactericidal activity.<sup>3</sup> Later, it was shown to have a range of pharmacological effects such as selectively blocking  $K^+$  channels<sup>4</sup> and promising anti-cancer activity through its ability to accumulate in mitochondria.<sup>5</sup> This can be explained by its two positive delocalized charges that can interact with the highly negative mitochondrial membrane.<sup>6,7</sup> As a result, it has been used as a mitochondrial targeting agent in the field of drug delivery and nanomedicine. DQ has been demonstrated to self-assemble in aqueous media and form nanoscaled structures

known as “DQasomes” that can be used to transport nucleic acids and drugs to mitochondria.<sup>8-12</sup> It has also been used to form “mitochondriotropic” liposomes carrying chemotherapeutic drugs, either by encapsulation<sup>13-16</sup> or by click-chemistry grafting onto the end of PEG chains.<sup>17</sup> Several papers have described its encapsulation in lipid nanocarriers for cancer therapy. Typically, these formulations carry 5 – 10 mol% of DQ. Thus, Weissig and co-workers described the formulation of micelles carrying DQ<sup>18</sup> and, more recently, DQA80, a lipid-based formulation (DOTAP/DOPE) has been reported to have anticancer potential, combining DQ targeting capacities and anticancer activities.<sup>19</sup> It has been clearly demonstrated that DQ was able to accumulate in cancer cells. Although DQ has also been shown to induce a loss of the mitochondrial transmembrane potential, to activate caspase-3 dependent pathways and to produce reactive oxygen species in prostate cancer cells (PC-3)<sup>20</sup> there is no clear information available about the nature of the interaction between DQ and the mitochondrial envelope, which is mainly composed of phosphatidylcholine ( $\approx 44\%$ ), phosphatidylethanolamine ( $\approx 34\%$ ), cardiolipin ( $\approx 14\%$ ) and phosphatidylinositol ( $\approx 5\%$ ).<sup>21</sup> In this study we have adopted a biophysical approach to study how DQ interacts with lipid bilayers as a model for its interaction with mitochondrial membranes and with lipid-based drug delivery systems. To this end, we have used two different lipid membrane systems. The first is liposomes of a composition that is often used for drug delivery<sup>22-24</sup> and mitochondrial targeting *in-vivo*<sup>13-15,17</sup> (egg PC, cholesterol and DSPE-PEG<sub>2000</sub> in 65:30:5 molar proportions). However, to obtain more detailed physicochemical data, DMPC bilayers were used as a simplified model of the outer mitochondrial membrane.<sup>21</sup>

## 2 Materials and methods

### 2.1 Chemicals

Chicken egg L- $\alpha$ -phosphatidylcholine (EPC), cholesterol (CH), the ammonium salt of 1,2-distearoyl-*sn*-glycero-3-phosphoethanolamine-*N*-[methoxy(polyethylene glycol)-2000] (DSPE-PEG<sub>2000</sub>), 1,2-dimyristoyl-*sn*-glycero-3-phosphocholine (DMPC) and 1,2-dimyristoyl-*sn*-glycero-3-phosphocholine deuterated on the two methylenes of the choline headgroup (DMPC-*d*<sub>4</sub>) were all purchased from Avanti Polar Lipids. Stock solutions of lipids (25 mg.mL<sup>-1</sup> for each) were prepared in chloroform. Dequalinium chloride (DQ) and Dulbecco's Phosphate Buffered Saline (without calcium chloride and magnesium chloride) were purchased from Sigma-Aldrich. Deuterium oxide and

water deuterium depleted were acquired from Eurisotop. Organic solvents (HPLC grade) were obtained from Carlo-Erba and used without further purification. Ultrapure water ( $\gamma = 72.2 \text{ mN.m}^{-1}$  at  $22^\circ\text{C}$ , resistivity  $18.2 \text{ M}\Omega.\text{cm}$ ) was produced by a Millipore Milli-Q Direct 8 water purification system.

## 2.2 *pKa determination for DQ.*

*In silico* pKa values of DQ have been calculated using Marvin Sketch software (ChemAxon). UV-spectrum of DQ were recorded at different pH in pure water (adjusted with NaOH or HCl 0.1 N) using a Perkin Elmer Lambda 25 spectrophotometer.

## 2.3 *Liposome preparation.*

Liposomes were prepared using the thin film rehydration method. Egg PC, Cholesterol, DSPE-PEG<sub>2000</sub> (in chloroform), 65:30:5 molar proportions respectively, together with different proportions of dequalinium (in methanol) were mixed in a round-bottomed flask and dried at  $25^\circ\text{C}$  using a rotary evaporator (R-215, Büchi, Switzerland) for 60 min. The film was then rehydrated with phosphate buffer solution (PBS) or water for 20 min to give a final lipid concentration of 25 mM. The multilamellar vesicles were then extruded through polycarbonate membranes using an extruder (Lipex<sup>TM</sup>, Northern Lipids, Canada); 3 times through  $0.2 \mu\text{m}$  pore size and 3 times through  $0.1 \mu\text{m}$  at  $25^\circ\text{C}$ . Liposomes were purified from non-associated DQ by centrifugation (10 min  $12,000 \text{ g}$ ) to remove visible aggregates and then by ultrafiltration using Amicon centrifugal filter unit with a molecular weight cut-off of 100 kDa (30 min;  $4,000 \text{ g}$ ;  $4^\circ\text{C}$ ), which retained the liposomes while allowing soluble unbound DQ molecules to pass. To study possible electrostatic interactions between DQ and the liposomal membrane, DQ ( $200 \mu\text{M}$  in pure water) was added to a pre-formed liposomal suspension (25 mM lipids) at room temperature and the mixture was vortexed for 2 min. DQ encapsulation efficiencies were determined by UV spectrophotometry (Perkin Elmer Lambda 25) at a wavelength of 326 nm.

## 2.4 *Size and $\zeta$ -potential measurements (Dynamic Light Scattering).*

The mean hydrodynamic diameter of the liposomes was determined by Dynamic Light Scattering (Zetasizer Nano ZS) (Malvern Instruments Corp., Worcestershire, UK). Samples were diluted 30-fold in pure water prior to measurement in a

disposable cuvette and analyzed at a backscatter angle of  $173^\circ$  and a temperature of  $25^\circ\text{C}$ . Polydispersity index (PDI) was used as an indicator of size distribution.  $\zeta$ -potential was measured using the same apparatus in a folded capillary cell after 30-fold dilution in pure water.

## 2.5 Sample preparation for physico-chemical studies.

Stock solutions of DMPC and dequalinium chloride were prepared by dissolving weighed amounts of dry powder in chloroform and methanol respectively. Binary mixtures were obtained by mixing appropriate amounts of the stock solutions and additional chloroform or methanol was added to reach a chloroform/methanol ratio of 2:1 (v/v). The samples were defined in terms of dequalinium content with  $r_{\text{DQ}} (\%) = 100 \times n_{\text{DQ}}/n_{\text{DMPC}}$ , where  $n_{\text{DQ}}$  and  $n_{\text{DMPC}}$  are expressed in moles. The organic DMPC/dequalinium chloride solutions were evaporated at room temperature under a gentle stream of nitrogen, followed by drying under a vacuum overnight in order to completely remove residual organic solvents. The dry lipid films were then hydrated by adding an appropriate amount of ultrapure water or phosphate buffer solution to reach a final content of 90% by weight and the samples were incubated at  $35^\circ\text{C}$  (a temperature above the phase transition temperature of the lipid) for 1 h with vigorous intermittent vortex mixing every 15 min. For  $^{31}\text{P}$  and  $^2\text{H}$  NMR spectroscopy, a 9:1 mixture of water and deuterium oxide, and pure deuterium-depleted water respectively were used instead of water to hydrate the films.

## 2.6 Differential scanning calorimetry (DSC).

DSC experiments were carried out using a Perkin-Elmer DSC Diamond apparatus equipped with an Intracooler 2P cooling device and connected to a Pyris Thermal Analysis Software System (version 9.1). The calorimeter was calibrated as described in IUPAC recommendations.<sup>25</sup> The samples (hydrated at 90% w/w with pure water or sterile-filtered phosphate buffer solution), in the range of 14–17 mg, were accurately weighed and hermetically sealed within 50  $\mu\text{L}$  aluminum pans (pan, part BO143017 and cover, part BO143003); an empty pan was used as a reference. The samples were cooled from  $55$  to  $-5^\circ\text{C}$  at a constant rate,  $|dT/dt| = 5^\circ\text{C}.\text{min}^{-1}$  and heated from  $-5$  to  $55^\circ\text{C}$  at different rates,  $dT/dt = 2, 3, 4$  and  $5^\circ\text{C}.\text{min}^{-1}$ . The first scan was preceded by a 10-min isotherm at  $25^\circ\text{C}$  to allow the samples to reach thermal



equilibrium. All the transitions were found to be reversible and reproducible in the repeated scans.

The transition temperatures were taken at the onset of the transitions ( $T_{\text{onset}}$ ) i.e., the intersection of the tangent to the left side of the endothermic peak with the baseline. The end temperature ( $T_{\text{end}}$ ), corresponding to the completion of transition, was also recorded. This temperature was taken at the intercept of the baseline with the tangent to the right-hand side of the heating curve. To eliminate the effects of the heating rate on the temperature, determinations were carried out at different rates, and the temperature was extrapolated to a zero rate. The transition enthalpy was determined from the area under the peaks and normalized by the phospholipid content. To calculate the area under the peak, a baseline connecting the linear segments of the heat capacity curve between the onset and endpoint of the transition was subtracted.

## 2.7 *Transmission electron microscopy combined with freeze fracture (FF-TEM).*

Approximately 2  $\mu\text{L}$  of each liposome dispersion were pipetted onto a gold sample holder, frozen by plunging immediately into partially solidified Freon (cooled by liquid nitrogen) for 20 s and stored in liquid nitrogen. Fracturing was performed at  $-100^\circ\text{C}$  in a Balzers freeze-fracture device (Balzers BAF 400D, Balzers AG, Liechtenstein). Replicas of the fractured faces etched at  $-100^\circ\text{C}$  were made by platinum shadowing and carbon coating and then cleaned with an aqueous solution of surfactant and washed with distilled water. The replicas were placed on 200 mesh copper grids and examined in a Morgagni 268D (FEI, The Netherlands) transmission electron microscope.

## 2.8 *Small- and wide-angle X-ray scattering measurements*

Small-angle X-ray scattering (SAXS) and wide-angle X-ray scattering (WAXS) experiments were performed at the BioSAXS/D beamline 4-2<sup>26</sup> of the Stanford Synchrotron Radiation Lightsource (SSRL) using a slit-collimated monochromatic X-ray beam with an X-ray energy of 12 keV ( $\lambda = 1.033 \text{ \AA}$ ). The sample solutions were loaded into a temperature controlled capillary flow cell. The capillary was housed inside an aluminum block thermally connected to two Peltier modules which provided fast temperature change in the  $5\text{--}40^\circ\text{C}$  range. For every temperature step the sample was equilibrated for 5 minutes inside the flow cell before X-ray data were



taken. After each sample the capillary was thoroughly cleaned before injecting the next sample to avoid cross contamination. The SAXS data were collected using a Dectris Pilatus3 X 1M detector (pixel size, 172  $\mu\text{m}$ ) at a sample-to-detector distance of 0.25 and 2.5 m (covering the scattering vector range of  $q = 0.05\text{--}2.0 \text{ \AA}^{-1}$  and  $0.005\text{--}0.39 \text{ \AA}^{-1}$ , respectively, where  $q = 4\pi \times \sin(\theta)/\lambda$  with  $2\theta$  being the scattering angle and  $\lambda$  the X-ray wavelength). Each sample was exposed 5 times to the X-ray beam for 0.5 s to record 2D SAXS patterns. To account for background scattering from the capillary and dispersion medium, the scattering intensity from the dispersion medium was subtracted from the scattering intensity from each sample solution. The scattering patterns were processed with the SasTool program (SasTool for Solution Data Analysis: <http://ssrl.slac.stanford.edu/~saxs/analysis/sastool.htm>) to integrate the intensity radially, subtract the buffer and sample cell background and generate averaged one-dimensional intensity ( $I(q)$ ) versus scattering vector ( $q$ ) profiles.

Fitting of the low  $q$ -regions of the SAXS data for extruded vesicles was carried out using the Global Analysis Program (GAP).<sup>27,28</sup> A symmetric model of a lipid bilayer in unilamellar vesicle was used for loaded liposomes in water, while a model of multilamellar lipid vesicles with a structure factor described by the paracrystalline theory for the gel phase and by the modified Caillé theory for the fluid phase was used for other SUVs. The electron density profiles were constructed from the best-fit results of the SAXS data and the respective bilayer thickness were calculated as described by Pabst et al..<sup>29</sup>

## 2.9 <sup>31</sup>P NMR spectroscopy.

<sup>31</sup>P NMR spectra were recorded on a Bruker AMX-400 spectrometer operating at 161.97 MHz using a dipolar echo sequence ( $\pi/2 - t - \pi - t$ ) with a spectral window of 64 kHz, a  $t$  value of 200  $\mu\text{s}$ , a  $\pi/2$  pulse of 13  $\mu\text{s}$ , a recycle delay of 2 s and a broadband proton decoupling during signal sampling by means of a Waltz-16 composite pulse sequence. Typically, 512 scans were recorded for phosphorus spectra with deuterium lock. A line broadening of 50 Hz was usually applied before Fourier transformation. Samples were allowed to equilibrate at least 1 min at a given temperature before the NMR signal was acquired; the sample temperature was regulated within 1°C by a BVT-1000 unit. Phosphoric acid (85%) was used as external reference.

### 2.10 Electron spin resonance spectroscopy.

Two DOXYL derivatives of stearic acid were added to membranes as spin labels: 5-DOXYL-stearic acid (5-DXA) and 16-DOXYL-stearic acid (16-DXA). Due to the position of the label, the former probes the superficial part of the membrane layer while the latter probes its hydrophobic core. Spin-labelled vesicles were prepared from the samples used for  $^{31}\text{P}$  NMR spectroscopy. Firstly, each sample was diluted to reach a DMPC concentration of 10 mM and was then sonicated to obtain SUVs. 100  $\mu\text{L}$  of each sample was then labelled with 2  $\mu\text{L}$  of a radical nitroxide-labelled probe solution (the concentrations, in DMSO, were equal to 5 mM and 1 mM for 5-DXA and 16-DXA respectively). After labelling and 30 min incubation at room temperature, each sample was transferred by capillarity into a 20  $\mu\text{L}$  Pyrex capillary tube and then inserted into the cavity of the spectrometer. Continuous-wave ESR spectra were recorded on a Bruker ESP 380 spectrometer at a frequency of 9.71 GHz at each temperature set by a variable temperature device over the temperature range from 20 to 40°C every 2°C. The complete membrane incorporation of the spin labels was ascertained by the absence on the spectra of the extremely resolved ESR lines corresponding to free rotating markers. Order parameters  $S$  were determined from the hyperfine splitting constants ( $2T_{\parallel}$  and  $2T_{\perp}$ ) measured on 5-DXA spectra, using the following relation  $S = 1.723 \times \frac{T_{\parallel} - T_{\perp} - C}{T_{\parallel} + 2 \times T_{\perp} + 2 \times C}$  with  $C = 1.4 - 0.053 \times (T_{\parallel} - T_{\perp})$ .<sup>30</sup> Rotational correlation times  $\tau_c$  were calculated from the peak-to-peak line width of the central line  $\Delta W_0$ , the peak height of the central line  $h_0$  and the peak height of the high-field line  $h_{-1}$  determined on 16-DXA spectra, using the following equation  $\tau_c = K \times \Delta W_0 \times \left( \sqrt{\frac{h_0}{h_{-1}}} - 1 \right)$  with  $K = 6.5 \times 10^{-10} \text{ s.G}^{-1}$ .<sup>31</sup>

### 2.11 $^2\text{H}$ NMR spectroscopy.

$^2\text{H}$  NMR spectra were recorded on a Bruker DMX-300 spectrometer operating at 46.07 MHz with a probe specifically designed for solid-state deuterium NMR experiments (Morris Instruments Inc., Gloucester Ontario, Canada). A quadrupolar echo sequence ( $\pi/2 - t - \pi/2 - t$ ) was used with a spectral width of 250 kHz, a  $t$  value of 40  $\mu\text{s}$ , a  $\pi/2$  pulse of 3.4  $\mu\text{s}$  and a recycle delay of 50 ms.<sup>32</sup> Typically, 20,000 scans were recorded for deuterium spectra. A zero-order phase correction was applied to obtain no signal in the imaginary channel. When necessary, the free

induction decay was shifted by a fraction of the dwell time using an orthogonal polynomial interpolation routine so that the Fourier transform could start at the top of the echo.<sup>33</sup> A line broadening of 10 kHz was then applied before Fourier transformation. The sample temperature was regulated to within 1°C by a BVT-2000 unit and allowed to equilibrate for at least 15 min after the temperature was stabilized, before the NMR signal was acquired. Spectrum deconvolution leading to oriented  $^2\text{H}$  NMR spectra ( $0^\circ$ ) were obtained numerically using the dePake-ing procedure.<sup>34</sup>

### 3 Results and discussion

#### 3.1 *pKa determination*

It was important to determine the pKa of DQ to ensure that the same molecular species were present in electrostatic binding studies performed in PBS and pure water (with pH values around 7.4 and 6 respectively). It was observed that the UV spectra of dequalinium remained unchanged at pH 2, pH 8 and pH 11, meaning that its molecular state remained the same over this range of pH (data not shown). However, pKa determinations of DQ are difficult to perform because of its low solubility in water; this explains why no clear value appears in the literature. Therefore, to complement our observation, in-silico pKa predictions were performed with Marvin Sketch software. These predictions showed a single species (" $\text{NH}_2\text{-NH}_2$ ") between pH 2 and pH 14, confirming the observations from UV spectrophotometry (Figure S1).

#### 3.2 *$\zeta$ -potential and size measurements*

Empty liposomes and liposomes containing 10% DQ were prepared using either water or PBS as the aqueous phase. Their surface charge was then investigated by  $\zeta$ -potential measurements. Under our experimental conditions, we observed a  $\zeta$ -potential of around -14 mV for empty liposomes made in PBS and -12 mV for liposomes made in water. The  $\zeta$ -potential for DQ-loaded liposomes was around -8 mV and 0 mV respectively in PBS and water. After 24 h of storage at 4 °C, no change in  $\zeta$ -potential was observed for liposomes prepared in water, whereas loaded liposomes made in PBS reverted to a  $\zeta$ -potential similar to that of empty liposomes (around -14 mV). Since all the samples were diluted by a constant factor of 30 before measurement, the difference in ionic strength between the preparations made

in water and in PBS was minimalized. More importantly, direct comparisons can be made between liposomes prepared under the same conditions with and without DQ and before and after storage.

Loaded liposomes made in water had a diameter of  $109 \pm 1$  nm whereas this was  $80 \pm 1$  nm for liposomes in PBS. Polydispersity indexes were found to be around 0.1 for both preparations meaning that the distributions were monodisperse (Figure 2).

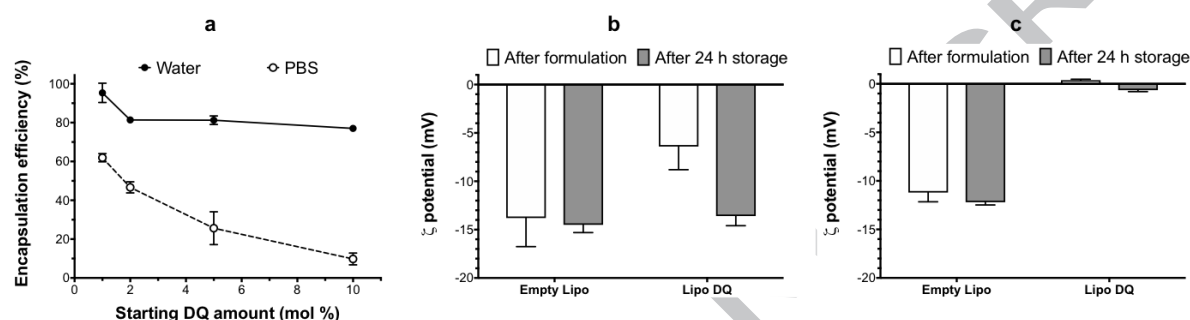


**Figure 2** Encapsulation efficiency of dequalinium in liposomes (eggPC/CH/DSPE-PEG<sub>2000</sub> 65/30/5) made in water or PBS after 24h of storage at 4°C (a). Liposomes were centrifuged (10 min; 10,000 g) and then ultrafiltrated to remove precipitated DQ prior to measurements.  $\zeta$ -potential variation of empty and DQ liposomes (10% of DQ) made in PBS (b) and water (c) immediately after preparation and after 24h of storage at 4°C. For these experiments, organic solutions of dequalinium and lipid mixture were dried to obtain a film that was then rehydrated and extruded to form small unilamellar vesicles. Values are mean of three independent experiments (mean  $\pm$  SD;  $n = 3$ ).

### 3.3 Retention of DQ in liposomes as a function of time

24 hours after formation of liposomes containing 10% DQ by thin film rehydration, those made in PBS were observed to have become exhibited a biphasic system, indicating their inherent instability. To investigate this further, several formulations were made in water and PBS at different DQ ratios. They were centrifuged (10 min; 10,000 g) 24h after formation to remove aggregates and the DQ remaining associated with the liposomes in the supernatant was determined by UV-spectrophotometry. As shown in Figure 2a, for DQ liposomes made in water, almost all the DQ initially incorporated was retained by the liposomes. In contrast, for liposomes made in PBS, at all DQ ratios, the proportion of retained DQ was lower

than that for liposomes made in water and decreased as the initial DQ content increased. This is evidence of leakage of DQ from liposomes when made in PBS and is consistent with the two phases observed in these preparations.

### 3.4 Electrostatic binding studies

To further investigate the differences between liposomes made in PBS and water, the ability of DQ to bind to preformed unloaded liposomes was studied. As shown in Figure 3a, when DQ was added to SUVs at different ratios, net increases in  $\zeta$ -potential were observed, indicating the association of this positively charged molecule at the surface. However, liposomes made in PBS showed smaller increases with increasing amounts of added DQ compared with liposomes formed in water. To see whether the presence of PEG chains influenced the binding of DQ,  $\zeta$ -potential variations on adding 10% DQ were measured in absence or presence of two different proportions of DSPE-PEG<sub>2000</sub> (the standard proportion of 5% and half this proportion) included in the membrane of liposomes prepared in water (Figure 3b).

No changes in  $\zeta$ -potential were observed for these three preparations, indicating that DQ preferentially binds to the polar headgroups of phospholipids rather than to the PEG chains. Finally, the association of externally added 10% DQ was studied in PBS or in water. In PBS, DQ did not remain associated with the liposomes (around 0% association) but in water almost 60% of DQ remained associated with the liposomes, suggesting a better affinity for the lipid bilayers in water (Figure 3c).

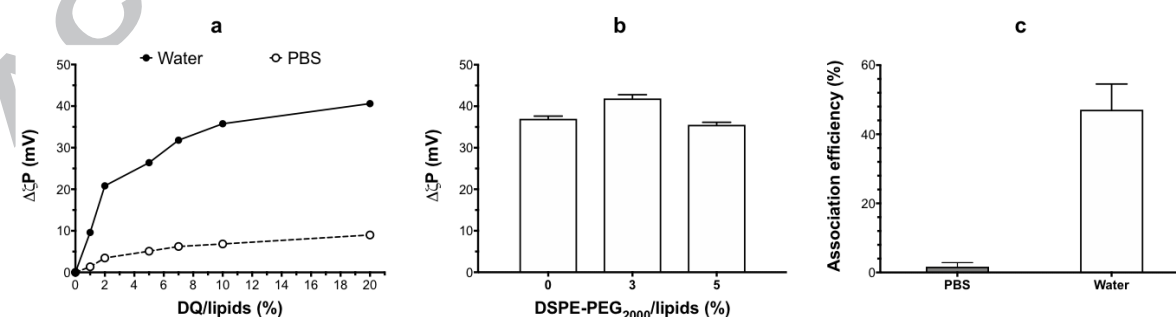


**Figure 3** Influence of DQ on  $\zeta$ -potential of after addition to pre-formed liposomes (eggPC/CH/DSPE-PEG<sub>2000</sub> 65/30/5) made in water (white circles) or PBS (black circles) (a). Influence of DSPE-PEG<sub>2000</sub> on  $\zeta$ -potential difference

after addition of 10% DQ (molar ratio) to empty liposomes with different proportions of DSPE-PEG<sub>2000</sub>.  $\Delta\zeta P = \zeta P(\text{liposomes} + 10\% \text{ DQ}) - \zeta P(\text{empty liposomes})$  (b). Association efficiency of 10% (molar ratio) DQ added to liposomes (eggPC/CH/DSPE-PEG<sub>2000</sub> 65/30/5) made in PBS (black) and in pure water (white) (c). Values are mean of three independent experiments (mean  $\pm$  SD;  $n = 3$ ).

### 3.5 Differential scanning calorimetry

To further investigate the interactions between DQ and membranes, DMPC model bilayers containing different ratios of DQ and rehydrated in either water or PBS were studied by DSC. We chose to use a synthetic phospholipid with a sharp phase transition for these studies in order to follow the influence of DQ more precisely. In pure water (Figure 4a), DSC heating recordings of DMPC vesicles containing DQ showed a change in the endotherm with respect to pure DMPC bilayers with a decrease in the area under curve of the pre-transition event and a decreased  $T_{\text{onset}}$  (9.9°C and 7.9°C for 1 and 2 mol% of DQ respectively; Figure 4b). A decrease in the transition enthalpy was observed; since it was found to be  $4.5 \pm 0.2 \text{ kJ.mol}^{-1}$  without DQ and  $1.3 \pm 0.2 \text{ kJ.mol}^{-1}$  and  $0.7 \pm 0.2 \text{ kJ.mol}^{-1}$  in presence of 1 and 2% DQ respectively (Figure 4c). For amounts of DQ above about 3 mol%, the thermal event relating to the pre-transition was not detected. In PBS (Figure S2), a disappearance of the pre-transition, detected at  $13.3 \pm 0.7^\circ\text{C}$  for pure DMPC, was observed over the whole range of DQ ratios tested in this study.

The incorporation of DQ into DMPC bilayers also reduced the onset temperature ( $T_{\text{onset}}$ ) of the main transition in water (Figure 4a) and to a less extent in a saline environment for high ratios of DQ (Figure S2). In PBS, the main transition temperature was unchanged in presence of 5% of DQ ( $24.0 \pm 0.2^\circ\text{C}$  vs.  $23.9 \pm 0.1^\circ\text{C}$  for pure DMPC) and slightly decreased to  $23.5 \pm 0.1^\circ\text{C}$  with 10% or 15% of DQ but in all cases the cooperativity of the transition remained unchanged since  $0.6^\circ\text{C}$  were needed to complete the transition in presence or in absence of DQ. Moreover, we observed no variation of the transition enthalpy since the molar enthalpy varied between  $25.1 \pm 0.8 \text{ kJ.mol}^{-1}$  without DQ and  $25.2 \pm 1.2 \text{ kJ.mol}^{-1}$  in the presence of DQ (whatever the ratio of DQ).

These variations confirmed the lack of interaction between DMPC chains and DQ. In water, for DQ ratios below around 2%, no clear variation of the main transition



temperature was observed without any alteration of the cooperativity. However, a small decrease in the enthalpy was found with a shift from  $24.8 \pm 0.3 \text{ kJ.mol}^{-1}$  without DQ to  $23.8 \pm 0.5 \text{ kJ.mol}^{-1}$  in the presence of DQ whatever the ratio of DQ (Figure 4c). Between 2 and 4 mol% of DQ, a small decrease in the main transition temperature was observed with a small lowering of the cooperativity and no variation of the molar enthalpy (about  $24.1 \pm 0.5 \text{ kJ.mol}^{-1}$ ). For higher ratios of DQ (above 4 mol%), a stabilization of the onset temperature of the main transition at  $22.7^\circ\text{C}$  (versus  $23.9^\circ\text{C}$  for pure DMPC) was noticed without any alteration of the cooperativity but also of the enthalpy with an enthalpy value of  $23.6 \pm 0.7 \text{ kJ.mol}^{-1}$  (vs.  $24.8 \pm 0.3 \text{ kJ.mol}^{-1}$  for pure DMPC).

One hypothesis to explain these observations is that DQ may not interact with the hydrophobic tails of lipids to any great extent and does not affect chain packing. The abolition of the pre-transition peak may be attributed to a preferential interaction with DMPC head groups, as already observed in the literature with poly(amidoamine) (PAMAM) dendrimers and dipalmitoylphosphatidylcholine (DPPC) bilayers.<sup>35</sup> Indeed, the pre-transition peak represents the conversion of a lamellar gel phase to a rippled gel phase; any modification of the space between polar head groups can prevent the transition between these two phases.<sup>36</sup>

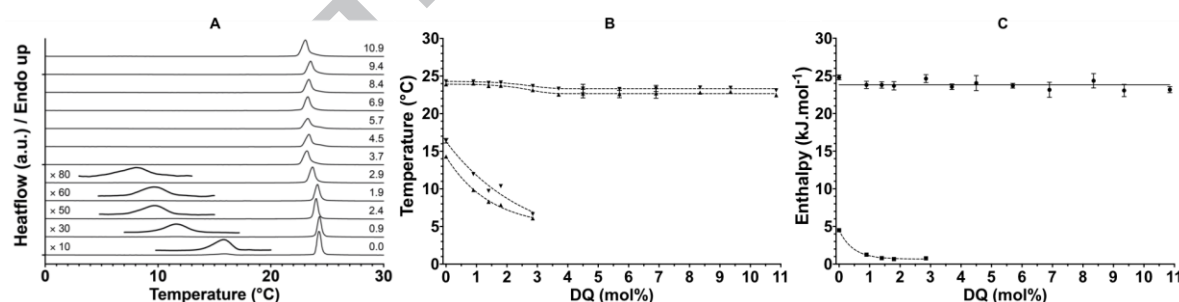


**Figure 4** DSC thermograms of fully hydrated (90% weight) DQ/DMPC mixtures in pure water (increasing ratios from bottom to top, the ratio was expressed in mol%) obtained at a rate of  $2^\circ\text{C.min}^{-1}$  during heating. The inserts show enlargements of the pre-transition (a). Variations as a function of DQ proportion of onset (▲) and endset (▼) temperatures (b) and enthalpies (c) of the pretransition (dotted line) and of the main transition (full line). Temperature uncertainties are obtained from the linear fit of temperatures (see experimental



part 2.6) and enthalpy values are mean of at least three experiments (mean  $\pm$  SD;  $n \geq 3$ ).

### 3.6 *Transmission Electron Microscopy combined with Freeze-Fracture (FF-TEM)*

Freeze-fracture TEM is a particularly useful tool for characterizing the morphology of lipid structures. FF-TEM of pure lipid systems provides information on lamellar lipid phases (e.g. size, shape and lamellarity), but can also reveal the structure of non-lamellar phases.<sup>37</sup> It is an especially appropriate technique for distinguishing multilamellar, unilamellar and non-lamellar lipid structures, yielding complementary information to other techniques (DSC, SAXS/WAXS).

DMPC bilayers rehydrated in absence of DQ show typical multilamellar liposomes (Figure 5a) with numerous adjacent bilayers. In presence of different ratios of DQ in water, a loss of multilamellar structures can be observed with the appearance of vesicular structures with only one bilayer (Figures 5b-5d) and clear boundaries typical of unilamellar vesicles. It is worth noting that for 1% DQ these objects coexist with multilamellar structures. With increasing ratios of DQ (2.5 and 5%) this coexistence is less prevalent. In PBS, the addition of 5% DQ did not change the aspect of bilayers, no clear difference can be observed between bilayers rehydrated in absence or presence of DQ (Figures 5e and 5f). These observations clearly reinforce the important role of the rehydration medium in the interaction between DQ and bilayers and the morphological changes confirm a stronger interaction in water. A probable explanation for the appearance of these unilamellar structures is the capacity of DQ to induce electrostatic repulsion between adjacent bilayers leading to membrane bending and, finally, to the formation of smaller unilamellar vesicles (with a size between 0.5 and 1  $\mu\text{m}$ ).

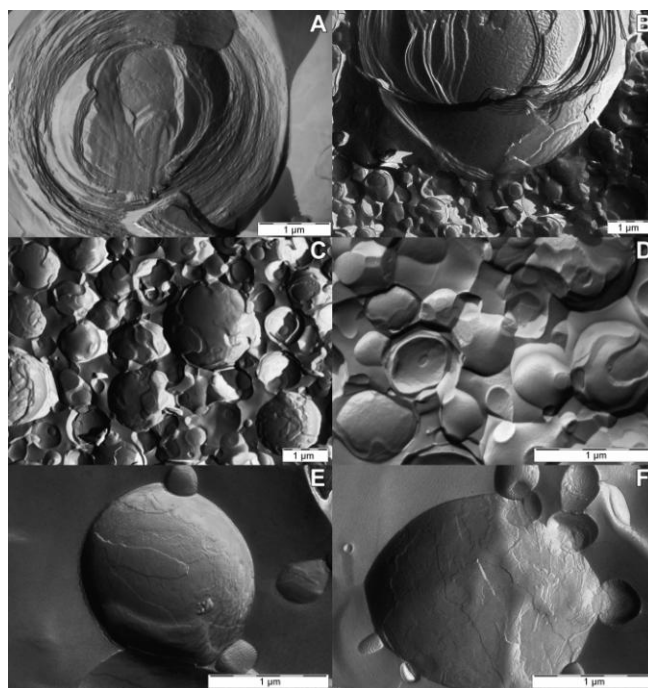


**Figure 5** FF-TEM images of DMPC membranes rehydrated in pure water (a, b, c, d) or in PBS (e, f) containing 0% (a, e), 1% (b), 2.5% (c) and 5% (d, f) of DQ. Scale bar represents 1  $\mu\text{m}$ .

### 3.7 Small- and wide-angle X-ray scattering

The influence of DQ on DMPC was further investigated by X-ray diffraction. Synchrotron SAXS/D and WAXS/D studies were performed on DMPC alone and DMPC containing 2.5, 5 and 10 mol% of DQ at several temperatures (from 5 to 40°C) in pure water (Figures 6 and S4). The SAXS pattern of a pure DMPC dispersion obtained at 5°C in water showed the presence of 6 broad Bragg peaks (the sixth order of diffraction was not observed), characteristic of a lamellar phase with a periodicity equal to 59.5 Å, which is in good agreement with the results published by Janiak et al. in 1979<sup>38</sup>, while the WAXS pattern displayed a narrow peak at  $q = 1.49 \text{ Å}^{-1}$  ( $d = 4.21 \text{ Å}$ ) together with a shoulder at  $q = 1.53 \text{ Å}^{-1}$  ( $d = 4.11 \text{ Å}$ ), characteristic of the distorted hexagonal chain organization in the phospholipid  $L_{\beta'}$  phase. At 15°C and 20°C, the WAXS patterns had only one symmetrical diffraction peak at  $q = 1.50 \text{ Å}^{-1}$  ( $d = 4.18 \text{ Å}$ ) indicating that the lipid chains were packed in a regular hexagonal lattice. Moreover, at 15°C and 20°C, the SAXS patterns were characteristic of the  $P_{\beta'}$  phase with a ripple length equal to 127.1 Å and 120.1 Å and with a lamellar distance of 65.0 Å and 64.9 Å, respectively. The lamellar distance and ripple wavelength

obtained at 20°C are quite similar to those obtained by Janiak et al.<sup>38</sup> or, more recently, by Wack and Webb.<sup>39</sup> The WAXS pattern for the  $L_\alpha$  phase, as would be expected, consists of a single broad diffuse reflection at  $q = 1.40 \text{ \AA}^{-1}$ , corresponding to a distance between the hydrocarbon chains close to 4.5 Å, indicative of the liquid state. SAXS patterns obtained at 30°C and 40°C showed two Bragg reflections characteristic of the  $L_\alpha$  phase with an interlamellar distance of 62.3 Å and 61.6 Å, respectively. Those values are in good agreement with the ones obtained by Pabst et al.<sup>29</sup> at lower hydration (75% w/w).

As can be seen in the SAXS patterns, the addition of 2.5 mol% of DQ to the DMPC system significantly changed the scattering patterns; causing a disappearance of the strong diffraction peaks and indicating loss of the smectic order of the DMPC bilayers, in both the gel phase and the fluid phase. This type of scattering pattern is consistent with that of unilamellar vesicles. A similar scattering pattern was observed for other systems with phospholipid bilayers in the absence of stacking; for example, in studies of mixed systems composed of the AT1 drug antagonist olmesartan and DPPC<sup>40</sup> or of the acidic form of the anti-cancer drug gemcitabine and DPPC.<sup>41</sup> This behaviour was observed with different ratios of DQ (from 1 to 15%) and at temperatures ranging from 0 to 50°C. This loss of binding may be attributed to electrostatic repulsion between adjacent membranes due to the positive charges of DQ. The first order diffraction peak is centered at  $q = 0.0154 \text{ \AA}^{-1}$ , corresponding to a d-spacing of about 410 Å, which is relatively large compared with pure DMPC vesicles, showing that the vesicles are highly swollen with water. During heating, in the gel phase, this behaviour was not modified but above the transition temperature, that is, in the fluid phase regime, a decrease in this distance was observed ( $d$  around 350 Å) and small and wide Bragg peaks, multiples of the low- $q$  peak, were observed. The addition of a larger proportion of DQ (5 mol%) did not fundamentally alter the phenomena observed with 2.5 mol% of DQ. However, a decrease in the interlamellar distance of about 40 Å in the gel phase and 20 Å in the fluid phase was observed. Moreover, a new Bragg peak appeared in the scattering pattern of the sample with 5 mol% of DQ at  $0.67 \text{ \AA}^{-1}$ . When the DQ content was further increased (10 mol%), no clear Bragg peak at low  $q$  could be observed at 5°C and 15°C and, for temperatures above or equal to 20°C, an interlamellar distance of about 300 Å could be determined. Furthermore, several Bragg peaks from crystalline DQ were visible at 10 mol%. Indeed, comparison with the diffraction pattern of the pure molecule (Figure

S3) demonstrated that all of the peaks coincided with those of crystalline DQ, showing a saturation of the bilayer with DQ for a content of about 5 mol%.

Below the phase transition temperature, irrespective of the amount of DQ, WAXS patterns showed only one symmetrical diffraction peak at  $q = 1.50 \text{ \AA}^{-1}$  indicating that the hydrocarbon chains of DMPC molecules were in a gel-state packing. When the samples were heated above the phase transition temperature, the DMPC molecules were in the fluid phase with a very broad WAXS peak at  $q = 1.40 \text{ \AA}^{-1}$ .

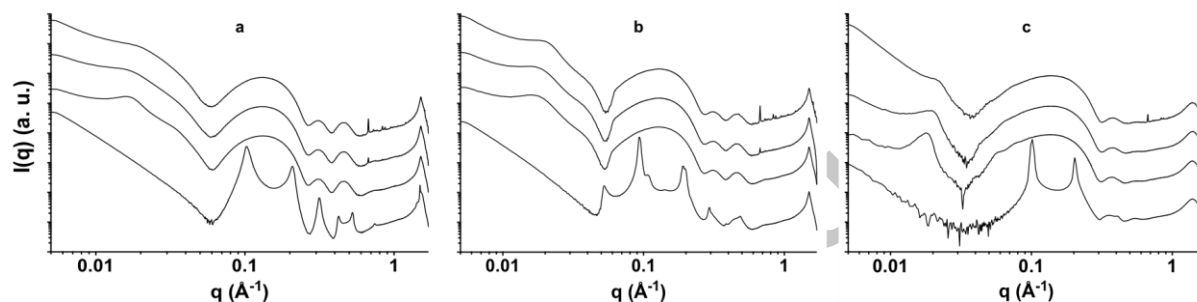


**Figure 6 SAXS and WAXS patterns of DMPC membranes in pure water containing different ratios of DQ (from bottom to top: 0, 2.5, 5 and 10 mol% of DQ) at 5°C (a), 20°C (b) and 40°C (c). For clarity, patterns are offset along the y-axis.**

In order to investigate the influence of ionic strength on vesicle behaviour, a SAXS/D study was performed on pure DMPC hydrated in presence of PBS (Figures 7 and S5). At low temperature (5°C), three broad Bragg peaks were observed with a constant periodicity between each peak, showing the presence of a  $L_{\beta'}$  phase with a lamellar distance equal to 59.8 Å. At intermediate temperatures (15°C and 20°C), a complex profile with many broad peaks was observed, indicating the formation of a ripple phase  $P_{\beta'}$ . Lamellar distances of 65.6 and 65.0 Å were determined at 15°C and 20°C respectively.

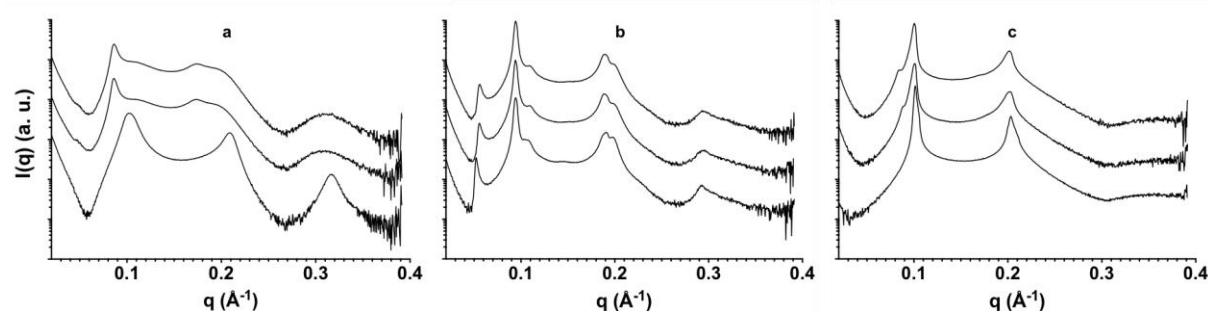


**Figure 7 SAXS patterns of DMPC membranes in PBS containing different ratios of DQ (from bottom to top: 0, 5 and 10 mol% of DQ) at 5°C (a), 20°C (b) and 40°C (c). For clarity, patterns are offset along the y-axis.**

The small peak at very low angles showed the ripple length of the  $P_{\beta'}$  phase to be 127.1 Å at 15°C. At higher temperature (20°C), this peak became more defined and the corresponding ripple wavelength decreased to 120.1 Å. At even higher temperatures (30°C and 40°C), only two narrower Bragg peaks were observed, indicating the formation of a  $L_{\alpha}$  phase with a lamellar distance equal to 63.0 Å and 61.8 Å respectively. In presence of 5% of DQ and at low temperature (5°C), a strange and broad pattern was observed that cannot be attributed to a  $L_{\beta'}$  (or  $L_{\beta}$ ) phase. Taking into account the first intense peak, a repeat distance of 64.4 Å was determined (presumably equal to the interlamellar distance). After heating the sample to 15°C, an additional Bragg peak at  $0.0537 \text{ Å}^{-1}$  was observed, which could be attributed to the (0,1) peak of the ripple phase  $P_{\beta'}$ . So, as a ripple phase was conspicuous at 15°C and since no phase transition was observed on the thermogram and because of the SAXS profile obtained at 5°C (especially the presence of a very low peak around  $0.05 \text{ Å}^{-1}$ ), we can envisage the formation of a ripple phase in presence of DQ at a lower temperature (below 0°C) than for pure DMPC. A similar result with a decrease of about 8°C of the temperature of interdigitated  $L_{\beta(i)}$  – ripple phase  $P_{\beta'}$  transition of ether-linked 1,2-dihexadecylphosphatidylcholine was observed in presence of 0.8 M of trehalose by Takahashi et al. in 1997.<sup>42</sup> From the first two Bragg peaks, a ripple wavelength and a lamellar distance equal to 117.1 Å and to 65.2 Å were determined respectively at 15°C. At 20°C, this Bragg peak was better defined, as for pure DMPC, and a lower ripple wavelength (112.6 Å) and a similar lamellar distance (64.8 Å) were observed. At higher temperatures, a  $L_{\alpha}$  phase with a lamellar distance equal to 63.5 Å was observed at 30°C but at 40°C a coexistence of two phases was detected, which could be attributed to the formation of a DQ-rich phase characterized by a higher lamellar distance (75.4 Å), due to the presence of dequalinium near the polar headgroup, and a second one with a lower lamellar distance (62.4 Å), very close to pure DMPC. Moreover, the same behavior was observed, and similar distances obtained, in presence of a higher ratio of DQ (10% of DQ).

In order to obtain more information about the interaction of dequalinium chloride and DMPC in a situation more comparable to liposomes used for drug delivery, small-angle X-ray scattering profiles were recorded on 100-nm extruded vesicles (Figure S6). In the case of pure DMPC membranes in water, one quasi-Bragg peak can be observed at 0.108 and 0.105 Å<sup>-1</sup> at 6 and 32°C respectively, showing the presence of about 7.5% of oligolamellar vesicles, mostly formed of two bilayers, in the sample. Similar behaviour was observed in PBS with the presence of a quasi-Bragg peak at 0.101 and 0.109 Å<sup>-1</sup> at 6 and 32°C respectively and an increase in the amount of bilamellar vesicles in the sample (about 9.2%). In water, the presence of 4.7 mol% of DQ (of the 5 mol% originally added) in the bilayer led to a pure diffuse scattering pattern of single and non-interacting bilayers. In PBS, the addition of DQ in the bilayer (about 0.8 mol% of the 5 mol% initially introduced) led to a decrease in the proportion of oligolamellar vesicles by a factor of two and a quasi-Bragg peak is only visible at 0.103 Å<sup>-1</sup> at 32°C. So, as a first conclusion, the addition of DQ tended to favour the formation of unilamellar structures. To go further with the analysis, electron density profiles were obtained from experimental data using the program GAP (Global Analysis Program), developed by Georg Pabst<sup>27,28</sup> and obtained from the author. In PBS, because of the small amount of encapsulated DQ, no clear difference in the electron density profiles could be observed and the same membrane thickness (taking into account the uncertainty) as for membranes without DQ was determined (Figures S8 and 8). In contrast, in pure water, a modification of the electron density profile was observed in presence of DQ, only at low temperature (Figures S7 and 8). Thus, an increase in the bilayer thickness of 3.2 Å could be detected at 6°C. It should be noted that the bilayer thickness of pure DMPC in water (46.3 Å at 32°C) is very close to the value found by Pabst et al. (46.8 Å at 30°C).<sup>29</sup>



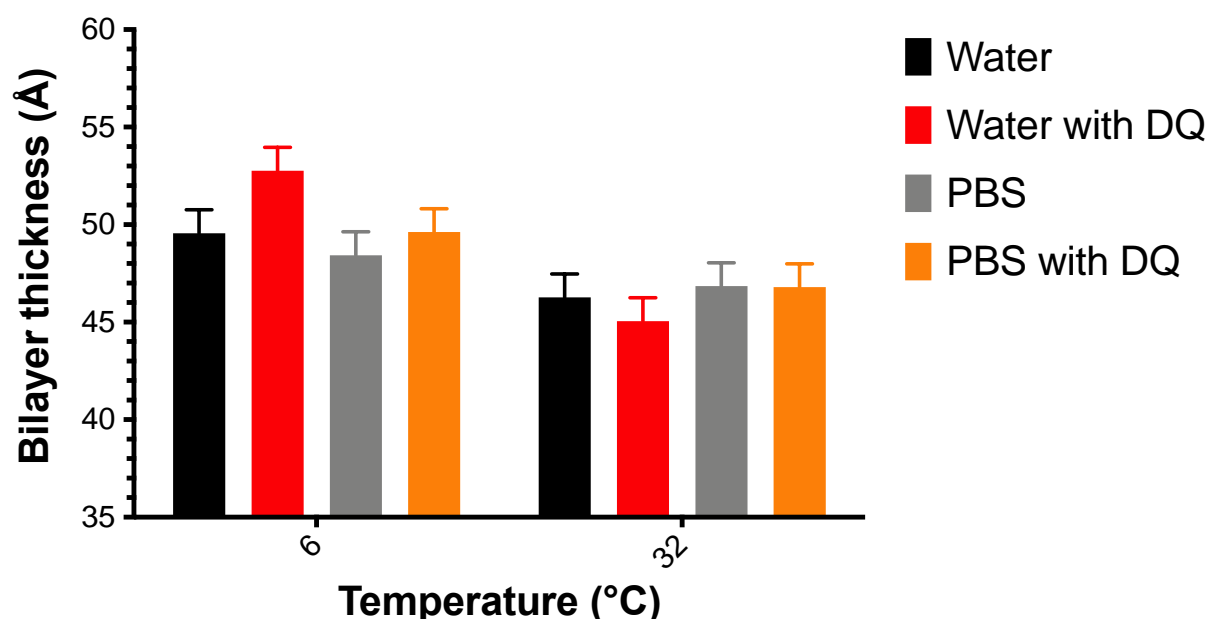


**Figure 8** Evolution of the bilayer thickness of DMPC membranes with or without DQ at 6°C or 32°C in pure water or in PBS. Bilayer thickness uncertainties are calculated from the fitting of SAXS profiles (see Figure S6).

### 3.8 $^{31}\text{P}$ NMR, ESR and $^2\text{H}$ NMR spectroscopy.

To verify the effect of DQ on DMPC polar head groups and to obtain some information about its location,  $^{31}\text{P}$  NMR studies were performed on pure DMPC bilayers and DMPC bilayers in presence of 1, 2.5, 5, 7.5 and 10 % of DQ in water. Typical static powder-like spectra were obtained, showing that the phospholipids were in a bilayer arrangement. Hence, the traces obtained at 6, 18 and 32°C for pure DMPC are similar to those obtained in the literature.<sup>43</sup> For DQ-containing bilayers at either ratio, no extra isotropic peaks were observed, which is in accordance with a unique phospholipid environment (Figures 9a-9c). The chemical shift anisotropy (CSA), which corresponds to the full width of NMR peaks and can be used to investigate polar head group mobility and related membrane fluidity, was determined and plotted as a function of temperature (Figures 9d and S9). The CSA values obtained for pure DMPC in the fluid phase are in accordance with the literature with a value around  $49 \pm 2$  ppm.<sup>44,45</sup> For pure DMPC, two CSA jumps were observed corresponding to the transition between the solid-ordered phase ( $L_{\beta'}$ ) and the ripple phase ( $P_{\beta}$ ) ( $T = 13^\circ\text{C}$ ) and to the transition between the ripple phase and the liquid-disordered phase ( $L_{\alpha}$ ) ( $T = 24^\circ\text{C}$ ). The addition of 1% of DQ led to the disappearance of the pre-transition and did not influence the temperature of the main phase



transition ( $T = 24^{\circ}\text{C}$ ,  $n = 3$ ), indicating that intermolecular interaction between the hydrocarbon tails of phospholipid molecules was unmodified by the presence of DQ. A decrease in CSA between 0 and  $13^{\circ}\text{C}$  (Figure 9d; at  $0^{\circ}\text{C}$ :  $90 \pm 1$  ppm for 1% DQ vs.  $98 \pm 1$  ppm for pure DMPC) and an increase in CSA in the fluid phase ( $53 \pm 2$  ppm at  $35^{\circ}\text{C}$ ) were observed in presence of 1% of DQ, indicating a fluidization of the solid-ordered phase and a rigidification of the liquid-disordered phase. Furthermore, the change in the lineshape of the  $^{31}\text{P}$  NMR for this sample, more specifically in the liquid-disordered phase, indicates a fragmentation of DMPC/DQ vesicles leading to a disparity of the vesicle sizes with coexistence of small unilamellar vesicles and larger vesicles, as previously observed by Traïka et al..<sup>46</sup> The addition of a higher proportion of DQ (between 2.5 and 10 %) to DMPC did not significantly influence either the temperature of the main phase transition ( $T = 23^{\circ}\text{C}$  for the four samples) or the CSA values for the fluid phase (CSA =  $52 \pm 1$  ppm at  $35^{\circ}\text{C}$ ) and the gel phase (CSA =  $88 \pm 1$  ppm at  $0^{\circ}\text{C}$ ). Since the CSA is directly related to reorientation of the polar head and the transition temperature to acyl chain packing, those results confirm a preferential interaction between DQ and phospholipid head groups.

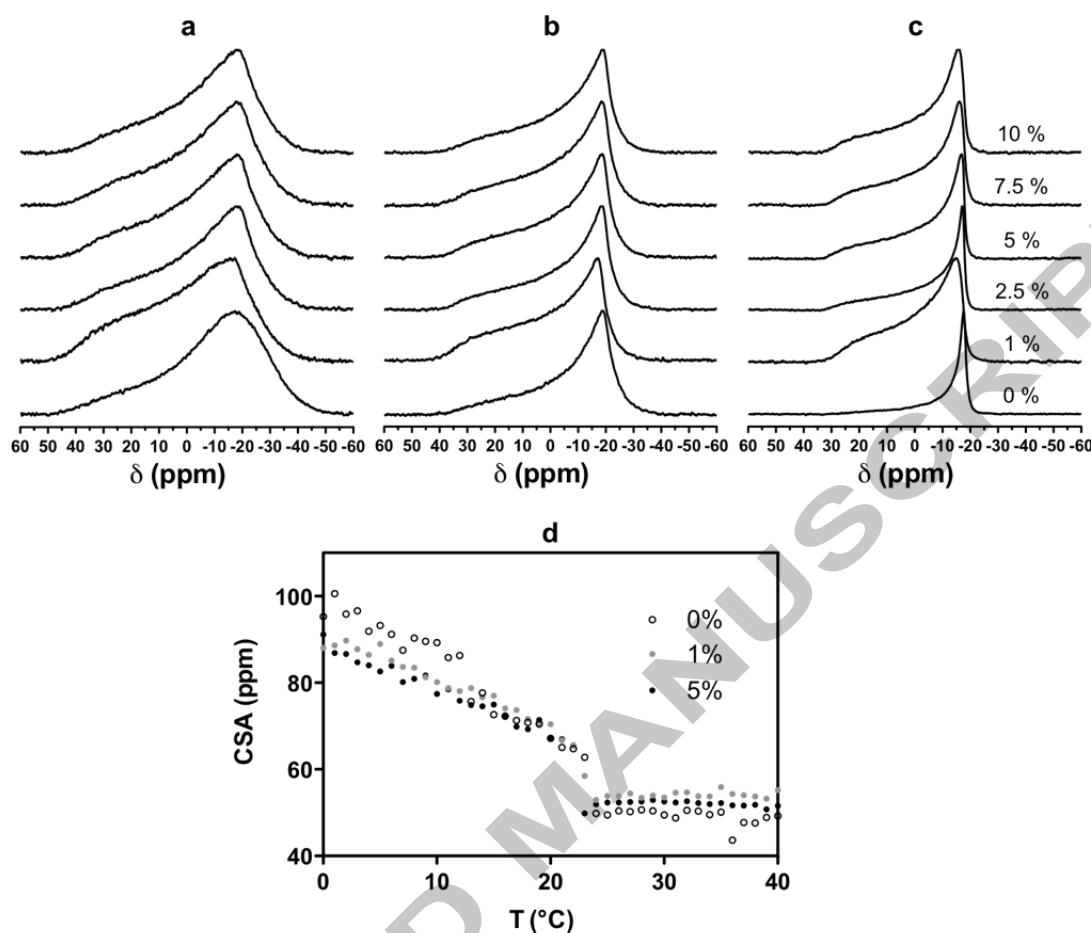


**Figure 9**  $^{31}\text{P}$ -NMR spectra of pure DMPC and DMPC containing between 1% and 10% of DQ in pure water at 6°C (a), 18°C (b) and 32°C (c). Panel d: chemical shift anisotropy (CSA) as a function of temperature of pure DMPC and DMPC containing 1% and 5% DQ.

In order to make sure that dequalinium was located near the head group of the phospholipids, electron spin resonance spectroscopy experiments using spin labels were carried out to investigate the membrane fluidity as a function of temperature. Two probes were used separately, 5-DOXYL-stearic acid (5-DSA) to give information about superficial membrane fluidity and 16-DOXYL-stearic acid (16-DSA) for the inner membrane region. With 5-DSA, two types of behaviour could be observed depending on the proportion of DQ (Figure S10). For DMPC alone or with a low ratio of DQ, similar curves were obtained: a relatively linear decrease of the order parameter  $S$  was observed when the temperature was increased. On the other hand, with a higher DQ content, a decrease of the order parameter  $S$  was first noticed at

the beginning of the temperature gradient; then, for high temperatures, the order parameter remained relatively constant and higher than that observed for lower proportions of DQ, showing a rigidification of the DMPC bilayer at high temperature in the presence of a high proportion of DQ. These phenomena were not observed when using a marker of the inner compartment of the membrane. Indeed, the results obtained with 16-DSA failed to show any difference in the rotational correlation time  $\tau_c$  of the probe as a function of DQ content at any temperature (Figure S11). These findings confirm that DQ was preferentially located near the phospholipid polar head.

To investigate the adsorption of DQ into the headgroup region of the membrane more closely,  $^2\text{H}$  NMR spectra of DQ-containing membranes prepared from DMPC with choline deuterated on the  $\alpha$  and  $\beta$  methylene groups (DMPC- $d_4$ ) were recorded. Analysis of the deuterium NMR spectra of deuterated headgroup phosphatidylcholines, allows conformational changes of the phosphocholine segment to be monitored, for example, as function of temperature,<sup>47</sup> for insertion of amphiphiles such as cholesterol,<sup>48</sup> membrane hydration,<sup>49</sup> or charge density at the membrane surface.<sup>50</sup> As in the  $^{31}\text{P}$  NMR studies, typical axially symmetrical  $^2\text{H}$  NMR spectra typical of phospholipids in a bilayer arrangement were obtained in the presence of various DQ concentrations at 37°C (Figure S12). Similarly, there is a slight heterogeneous line broadening of the NMR spectra recorded at low DQ proportions, reflecting the sample disparity resulting from the partial fragmentation of the DMPC multilamellar liposomes into smaller vesicular aggregates, as shown by freeze-fracture (Figure 5). Figure 10a shows the deconvoluted (DePaked) traces obtained from these powder spectra, allowing a precise measurement of the two-observed deuterium quadrupolar splittings attributed to the  $\alpha$  and  $\beta$   $\text{CD}_2$  methylene groups of the choline headgroups. In the absence of DQ, the splitting is larger for the  $\alpha$  deuterons (12.7 kHz) than for the  $\beta$  deuterons (10.4 kHz). The linewidth of the former is also larger due to a slight inequivalence of the  $\alpha$  deuterons. The assignment of the choline  $\alpha$  and  $\beta$  quadrupolar splittings were deduced from previous studies with DMPC deuterated specifically at the  $\alpha$  or  $\beta$  positions,<sup>51</sup> and from their temperature dependence,<sup>47,48</sup> where the  $\beta$  splitting is known to decrease upon heating, while the  $\alpha$  splitting remains constant (Figure S13). The two splittings coalesce upon addition of 1% DQ and are resolved again with 3% DQ. Based on their temperature dependence (Figure S13), we can assign the larger splitting at 3%

DQ to the  $\beta$  deuterons, indicating in fine that the DQ binding to the DMPC membranes induces an increase and a decrease, respectively, of the  $\beta$  and  $\alpha$  quadrupolar splittings. Similar, although smaller variations are obtained with 5% DQ, a concentration above which the effect induced by DQ on the choline headgroup appears to reach a plateau as confirmed by the spectrum recorded with 10% DQ. These results are summarized in Figure 10b showing the DQ concentration dependence of the choline  $\alpha$  and  $\beta$  quadrupolar splittings, revealing a clear saturation of the choline perturbation above 5% DQ.

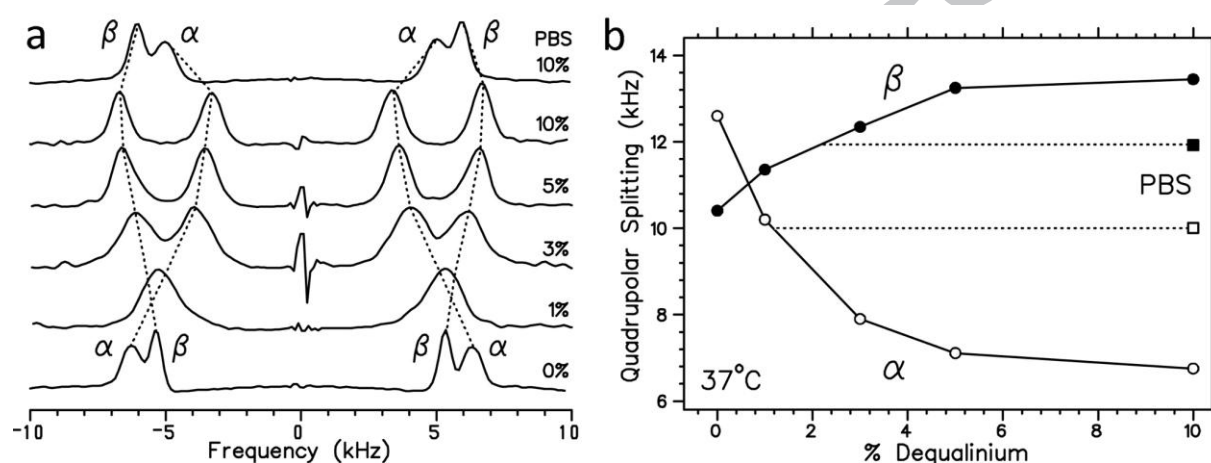


**Figure 10 (a)  $^2\text{H}$ -NMR DePaked spectra of DMPC- $d_4$  membranes in pure water at pH 7 or in PBS recorded at 37°C with 0%, 1%, 3%, 5%, 10% of DQ. (b) Dequalinium concentration dependence of the quadrupolar splittings of the choline  $\alpha$  (○, □) and  $\beta$  (●, ■) methylene deuterons measured on the NMR spectra of panel (a), in pure water (●, ○) or PBS (■, □).**

The analysis of the two curves indicates that the amplitude of the  $\alpha$  decrease is about twice that of the  $\beta$  increase. This pattern is typical of a conformational change of the choline headgroup induced by the insertion of a cationic layer of charges at the membrane surface. This latter effect is due to a well-known property of the phosphocholine dipole formed between the negatively charged phosphorus and positively charged quaternary ammonium groups, which acts as a “molecular electrometer” sensitive to the sign and the density of the membrane smeared surface charge<sup>50</sup>. According to the well-established model developed from 1981 by J. Seelig<sup>47</sup>, M. Bloom<sup>52</sup> and P. McDonald<sup>50</sup>, the  $\alpha$  splitting decreases or increases upon

membrane adsorption of cationic or anionic charges respectively, while the  $\beta$  splitting varies in the opposite sense to the  $\alpha$  splitting. For instance, it has been shown<sup>52</sup> that the binding of metallic cations such as  $\text{Ca}^{2+}$  to phosphatidylcholine membranes induces an effect which is similar to that observed here with DQ, while the incorporation in the bilayers of negatively charged phosphatidylserine induces the opposite effect, that is a decrease and an increase of, respectively, the  $\alpha$  and  $\beta$  quadrupolar splittings. Thus, the choline response observed in the presence of the positively charged cation  $\text{DQ}^{2+}$  to our DMPC membranes, is a clear indication of its adsorption at the membrane surface, with the cationic aromatic cycle located similarly to  $\text{Ca}^{2+}$ , at the bottom of the headgroup region.<sup>51,52</sup> A more comprehensive study of the DQ/DMPC system, which will be published elsewhere, suggests that the response of the phosphocholine “molecular electrometer” to the layer of DQ charges at saturation is actually equivalent to that induced by the cationic layer of membrane bound  $\text{Cd}^{2+}$  ions on phosphatidylcholine headgroups.<sup>47</sup>

Finally, we investigated the choline response to 10% DQ with membranes prepared in PBS. As shown on Figures 10a and 10b, the response observed at this concentration is smaller in the presence of PBS than in pure water, giving  $\alpha$  and  $\beta$  splitting values around those observed with 1% DQ in water, confirming that DQ binding to DMPC membranes is attenuated in PBS.

### 3.9 Modelization of possible interactions between DQ and lipid membranes

Taking all our experimental data together, we have created a tentative model of the interactions between DQ and lipid bilayers (Figure 11). Using a variety of techniques, we found DQ can interact better with bilayers rehydrated in water than in saline medium. Moreover, we also found DQ was able to interact with polar head groups, independently of the presence of PEG, in water due to its two delocalized positive charges, as indicated by the large variations in  $\zeta$ -potential that were observed (Figures 2c and 3a). In an ionic medium like PBS, we found that DQ did not remain associated with the surface of empty liposomes (Figure 3c). Thus, electrostatic binding of DQ to negatively charged lipid head groups seems to be the driving force for its encapsulation during film formation. Together with DSC studies, NMR experiments suggest a strong interaction with polar head groups in water (disappearance of the pre-transition), and a low interaction with hydrophobic chains

meaning that chain packing was not strongly disturbed (Figures 4 and 6). We can then assume a “U-shape” insertion of dequalinium in the bilayer more than a fully extended membrane-spanning insertion, due to a poor incorporation capacity and strong electrostatic interactions with polar head groups (Figure 11).

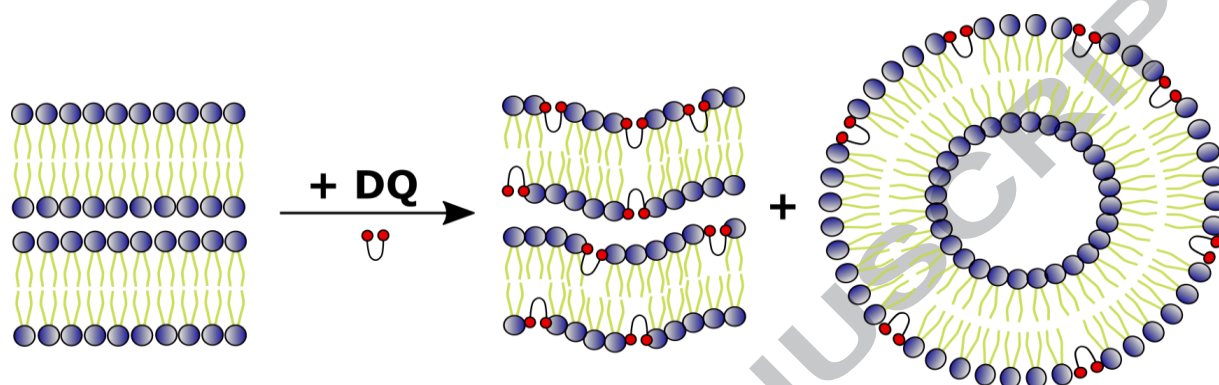


**Figure 11 Sketch of probable insertion of DQ in a lipid bilayer. DQ may induce membrane repulsion due to electrostatic interactions with negatively charged polar head groups of two adjacent bilayers in water leading to the formation of vesicles.**

In fact, symmetrical molecules separated by a saturated hydrocarbon chain tend to adopt this conformation in lipid environments.<sup>54</sup> Moreover, Monte-Carlo simulations of DQAsomes showed the coexistence of stretched and horseshoe (U-shape) conformations of DQ, the proportion between these two conformations being highly temperature-dependent.<sup>55</sup>  $^{31}\text{P}$  and  $^2\text{H}$  NMR studies confirmed a preferential interaction between DQ and polar head groups in the fluid phase but also an effect on the pre-transition (Figure 9). In addition, the DSC, WAXS/D and  $^2\text{H}$  NMR experiments confirmed the maximum incorporation of DQ in the bilayer in pure water to be around 5 mol%. Moreover, complex SAXS patterns obtained in water revealed possible attraction/repulsion phenomena between bilayers containing DQ despite a conserved lamellar structure seen with  $^{31}\text{P}$  and  $^2\text{H}$  NMR experiments. Furthermore, the  $^2\text{H}$  NMR experiments demonstrate unequivocally, that  $\text{DQ}^{2+}$  is closely bound at the surface of the zwitterionic DMPC membranes. All these results suggest that encapsulation of DQ in liposomes should be performed in water rather than strong ionic media for better stability. The difficulty of incorporating DQ in liposomes in ionic



media could be due to the phenomena of Debye screening or the formation of "salt-bridges" between DQ and anionic buffer components. This is exemplified in the work of Weissig et al. in which they briefly stated they could not incorporate DQ in liposomes at "physiological salt concentrations"<sup>18</sup>. Lower encapsulation efficiencies of DQ in PBS compared with pure water together with unchanged main transition temperature observed in PBS clearly indicate a weak electrostatic interaction between DQ and lipid bilayers. This has also been seen for the interaction of some antimicrobial peptides and DMPC model membrane.<sup>56</sup> In several other published studies, DQ-based liposomes were used to deliver anthracyclines<sup>14-16</sup> or topotecan<sup>13</sup> which can be incorporated by remote loading. This technique requires the use of ammonium sulfate (250 mM) as a rehydration buffer which may not guarantee an optimal encapsulation efficiency of DQ or good stability over time due to high ionic strength. It should be borne in mind that using deionized water as the suspension medium is not suitable for intravenous injection because of osmotic unbalance with physiological osmolality (290 mOsmol.kg<sup>-1</sup>).<sup>57</sup> Therefore, salt-free isotonic solutions such as 5% dextrose or 10% sucrose can be suggested as the hydration medium but the ionic strength will necessarily rise after mixing with physiological fluids, leading to loss of DQ.<sup>58</sup> Consequently, alternative approaches for mitochondrial targeting with lipid systems can be recommended; for example, the use of other targeting molecules such as peptides like mitochondria penetrating peptide (MPP)<sup>59</sup> or TPP that can be stably inserted in lipid bilayers when conjugated with a stearyl group (STPP)<sup>60</sup> or using DQ at the end of the PEG chain as previously described with liposomes encapsulating resveratrol<sup>17</sup>. FF-TEM experiments also revealed DQ was able to form vesicles from bilayers. A probable explanation for this phenomenon is membrane swelling and bending due to electrostatic repulsion. The profound change in the SAXS profiles suggests that DQ was inserted into the lipid bilayers. Since DMPC is zwitterionic it is likely that DQ interacts with the negative charge on the phosphate group, favoring insertion into the bilayer. Indeed, electrostatic interactions also occur with zwitterionic membranes, for example, divalent cations such as Ca<sup>2+</sup> or Cd<sup>2+</sup> are able to bind pure phosphatidylcholine membranes without any anionic lipids.<sup>47,52</sup> The <sup>2</sup>H NMR experiments indicate clearly that DQ<sup>2+</sup> interacts with DMPC bilayers in a similar way.

Another reason for the observed liposome fragmentation could be the generation of a positive curvature in the outer leaflet of the membrane due to the "U-shaped"



insertion of DQ at the interface, as observed upon insertion of non-cylindrical inverted cone-shaped amphiphilic molecules into the bilayer. If any, this curvature effect is probably not the main driving force for the fragmentation of multilamellar liposomes, and electrostatic interaction must be also involved. The adsorption of cationic DQ<sup>2+</sup> at the membrane surface in pure water is expected to induce electrostatic-driven repulsion between the bilayers, loosening the multilamellar structure and also allowing its fragmentation into smaller lipid vesicles.

#### 4 Conclusions

In this paper, we have investigated the feasibility of using DQ-loaded liposomes as a mitochondrial targeting agent. Indeed, in the literature, several studies of mitochondriotropic liposomes encapsulating chemotherapeutics revealed interesting results, suggesting new strategies for cancer therapy. For example, some targets involved in the cancer disease such as hsp90 have isoforms localized in the mitochondria, leading to growing interest in specific targeting of this organelle.<sup>53</sup> However, the interaction between DQ and lipid bilayers has never been discussed in the literature. Our results indicate that this interaction depends strongly on the ionic strength and that the association would be unstable in physiological salt condition. This work paves the way for further studies to reconsider the formulation of DQ-based nanomedicines and, more generally, on how positively charged lipophilic compounds can accumulate within and interact with mitochondrial membranes. In this context, it would be interesting to study mixed membranes of PC with an anionic lipid, with which we would anticipate a stronger DQ binding, even in the presence of PBS. These results would give further insights into the mechanism occurring at the level of the mitochondrial envelope where DQ accumulates and exerts its anticancer activity.

#### Acknowledgements

Use of the Stanford Synchrotron Radiation Lightsource, SLAC National Accelerator Laboratory, is supported by the U.S. Department of Energy, Office of Science, Office of Basic Energy Sciences under Contract No. DE-AC02-76SF00515. The SSRL Structural Molecular Biology Program is supported by the DOE Office of Biological and Environmental Research, and by the National Institutes of Health, National Institute of General Medical Sciences (including P41GM103393). The contents of this

publication are solely the responsibility of the authors and do not necessarily represent the official views of NIGMS or NIH. The authors thank Dr Georg Pabst (University of Graz, Graz, Austria) for providing GAP code to analyze SAXS data, Dr Benjamin Abecassis (LPS, UMR CNRS 8502, France) for his help in acquiring the preliminary SWAXS profiles, Frédéric Bourbon (IRBA) for the acquisition of ESR spectra, Teréz Kiss (RCNS, HAS) for FF-TEM investigations, Dr Sylviane Lesieur (IGPS, UMR CNRS 8612, France) for her advice about the determination of pKa, Pr Bernard Masereel (University of Namur, Belgium) for his attempt to determine the pKa of DQ, Dr Claudie Bourgaux (IGPS, UMR CNRS 8612, France) for fruitful discussions. Félix Sauvage received a grant from the French MESR.

## References

- 1) R.K. Naviaux, *Mitochondrion* **2004**, 4, 351–361.
- 2) M. Babbs, H.O. Collier, W.C. Austin, M.D. Potter, E.P. Taylor, *J. Pharm. Pharmacol.* **1956**, 8, 110–119.
- 3) V. Della Casa, H. Noll, S. Gonser, P. Grob, F. Graf, G. Pohlig, *Arzneimittelforschung*. **2002**, 52, 699–705.
- 4) N.A. Castle, D.G. Haylett, J.M. Morgan, D.H. Jenkinson, *Eur. J. Pharmacol.* **1993**, 236, 201–207.
- 5) M.J. Weiss, J.R. Wong, C.S. Ha, R. Bleday, R.R. Salem, G.D. Steele, L.B. Chen, *Proc. Natl. Acad. Sci.* **1987**, 84, 5444–5448.
- 6) V. Weissig, *Pharm. Res.* **2011**, 28, 2657–2668.
- 7) R.K. Pathak, N. Kolishetti, S. Dhar, *Wiley Interdiscip. Rev. Nanomed. Nanobiotechnol.* **2015**, 7, 315–329.
- 8) B. Vaidya, A.K. Goyal, K. Khatri, N. Mishra, R. Paliwal, S. Rai, S. Tiwari, S. Vyas, *Int. J. Biomed. Nanosci. Nanotechnol.* **2010**, 1, 95–108.
- 9) V. Weissig, J. Lasch, G. Erdos, H.W. Meyer, T.C. Rowe, J. Hughes, *Pharm. Res.* **1998**, 15, 334–337.
- 10) V. Weissig, V.P. Torchilin, *J. Drug Target.* **2001**, 9, 1–13.
- 11) G.G. D'Souza, R. Rammohan, S.M. Cheng, V.P. Torchilin, V. Weissig, *J. Control. Release* **2003**, 92, 189–197.
- 12) Š. Zupančič, P. Kocbek, M.G. Zariwala, D. Renshaw, M.O. Gul, Z. Elsaid, K.M. Taylor, S. Somavarapu, *Mol. Pharm.* **2014**, 11, 2334–2345.
- 13) Y. Yu, Z.H. Wang, L. Zhang, H.J. Yao, Y. Zhang, R.J. Li, R.J. Ju, X.X. Wang, J. Zhou, N. Li, W.L. Lu, *Biomaterials* **2012**, 33, 1808–1820.
- 14) L. Zhang, H.J. Yao, Y. Yu, Y. Zhang, R.J. Li, R.J. Ju, X.X. Wang, M.G. Sun, J.F. Shi, W.L. Lu, *Biomaterials* **2012**, 33, 565–582.
- 15) Y. Men, X.X. Wang, R.J. Li, Y. Zhang, W. Tian, H.J. Yao, R.J. Ju, X. Ying, J. Zhou, N. Li, L. Zhang, Y. Yu, W.L. Lu, *Int. J. Nanomedicine* **2011**, 6, 3125–3137.
- 16) L. Liu, L.M. Mu, Y. Yan, J.S. Wu, Y.J. Hu, Y.Z. Bu, J.Y. Zhang, R. Liu, X.Q. Li, W.L. Lu, *Int. J. Nanomedicine* **2017**, 12, 4163–4176.
- 17) X.X. Wang, Y.B. Li, H.J. Yao, R.J. Ju, Y. Zhang, R.J. Li, Y. Yu, L. Zhang, W.L. Lu, *Biomaterials* **2011**, 32, 5673–5687.
- 18) V. Weissig, C. Lizano, V.P. Torchilin, *J. Liposome Res.* **1998**, 8, 391–400.

- 19) Y. Bae, M.K. Jung, S. Lee, S.J. Song, J.Y. Mun, E.S. Green, J. Han, K.S. Ko, J.S. Choi, *Eur. J. Pharm. Biopharm.* **2018**, 124, 104-115.
- 20) K. Makowska, M.C. Estañ, I. Gañán-Gómez, M.C. Boyano-Adánez, A.I. García-Pérez, P. Sancho, *Mol. Biol.* **2014**, 48, 359–370.
- 21) S.E. Horvath, G. Daum G., *Prog. Lipid Res.* **2013**, 52, 590-614.
- 22) F. Sauvage, S. Franzè, A. Bruneau, M. Alami, S. Denis, V. Nicolas, S. Lesieur, F.-X. Legrand, G. Barratt, S. Messaoudi, J. Vergnaud-Gauduchon, *Int. J. Pharm.* **2016**, 499, 101–109.
- 23) F. Sauvage, E. Fattal, W. Al-Shaer, S. Denis, E. Brotin, C. Denoyelle, C. Blanc-Fournier, B. Toussaint, S. Messaoudi, M. Alami, G. Barratt, J. Vergnaud-Gauduchon, *Cancer Lett.* **2018**, 432, 103-111.
- 24) S. Maillard, T. Ameller, J. Gauduchon, A. Gougelet, F. Gouilleux, P. Legrand, V. Marsaud, E. Fattal, B. Sola, J.-M. Renoir, *J. Steroid Biochem. Mol. Biol.* **2005**, 94, 111–121.
- 25) G. Della Gatta, M.J. Richardson, S.M. Sarge, S. Stølen, *Pure Appl. Chem.* **2006**, 78, 1455-1476.
- 26) I.L. Smolsky, P. Liu, M. Niebuhr, K. Ito, T.M. Weiss, H. Tsuruta, *J. Appl. Crystallogr.* **2007**, 40, s453–s458.
- 27) G. Pabst, M. Rappolt, H. Amenitsch, P. Laggner, *Phys. Rev. E* **2000**, 62, 4000–4009.
- 28) G. Pabst, R. Koschuch, B. Pozo-Navas, M. Rappolt, K. Lohner, P. Laggner, *J. Appl. Crystallogr.* **2003**, 36, 1378–1388.
- 29) G. Pabst, J. Katsaras, V.A. Raghunathan, M. Rappolt, *Langmuir* **2003**, 19, 1716–1722.
- 30) B.M. Sefton, B.J. Gaffney, *J. Mol. Biol.* **1974**, 90, 343–358.
- 31) A. Keith, G. Bulfield, W. Snipes, *Biophys. J.* **1970**, 10, 618–629.
- 32) J.H. Davis, K.R. Jeffrey, M. Bloom, M.I. Valic, T.P. Higgs, *Chem. Phys. Lett.* **1976**, 42, 390–394.
- 33) J.H. Davis, *Biochim. Biophys. Acta* **1983**, 737, 117–171.
- 34) E. Sternin, M. Bloom, A.L. Mackay, *J. Magn. Reson.* **1983**, 55, 274–282.
- 35) K. Gardikis, S. Hatziantoniou, K. Viras, M. Wagner, C. Demetzos, *Int. J. Pharm.* **2006**, 318, 118–123.
- 36) B. Klajnert, J. Janiszewska, Z. Urbanczyk-Lipkowska, M. Bryszewska, R.M. Epand, *Int. J. Pharm.* **2006**, 327, 145–152.

- 37) H.W. Meyer, W. Richter, *Micron* **2001**, 32, 615–644.
- 38) M.J. Janiak, D.M. Small, G.G. Shipley, *J. Biol. Chem.* **1979**, 254, 6068–6078.
- 39) D.C. Wack, W.W. Webb, *Phys. Rev. A* **1989**, 40, 2712–2730.
- 40) D. Ntountaniotis, G. Mali, S.G. Grdadolnik, H. Maria, A.L. Skaltsounis, C. Potamitis, E. Siapi, P. Chatzigeorgiou, M. Rappolt, T. Mavromoustakos, *Biochim. Biophys. Acta* **2011**, 1808, 2995–3006.
- 41) B. Pili, C. Bourgaux, F. Meneau, P. Couvreur, M. Ollivon, *J. Therm. Anal. Calorim.* **2009**, 98, 19–28.
- 42) H. Takahashi, H. Ohmae, I. Hatta, *Biophys. J.* **1997**, 73, 3030–3038.
- 43) E.J. Dufourc, C. Mayer, J. Stohrer, G. Althoff, G. Kothe, *Biophys. J.* **1992**, 61, 42–57.
- 44) I.C.P. Smith, I.H. Ekiel, in *Phosphorous-31 NMR: Principles and Applications* Ed. D.G. Gorenstein, Academic Press, Orlando, **1984**, 15, 447–475.
- 45) S. Rajan, S.Y. Kang, H.S. Gutowsky, E. Oldfield, *J. Biol. Chem.* **1981**, 256, 1160–1166.
- 46) M. Traïkia, D.E. Warschawski, M. Recouvreux, J. Cartaud, P.F. Devaux, *Eur. Biophys. J.* **2000**, 29, 184–195.
- 47) H. Akutsu, J. Seelig, *Biochemistry* **1981**, 20, 7366–7373.
- 48) M.F. Brown, J. Seelig, *Biochemistry* **1978**, 17, 381–384.
- 49) B. Bechinger, J. Seelig, *Phys. Lipids* **1991**, 58, 1–5.
- 50) P.M. Macdonald, *Acc. Chem. Res.* **1997**, 30, 196–203.
- 51) M. Roux, J.M. Neumann, R.S. Hodges, P.F. Devaux, M. Bloom, *Biochemistry* **1989**, 28, 2313–2321.
- 52) M. Roux, M. Bloom, *Biochemistry* **1990**, 29, 7077–7089.
- 53) F. Sauvage, S. Messaoudi, E. Fattal, G. Barratt, J. Vergnaud-Gauduchon, *J. Controlled Release* **2017**, 248, 133–143.
- 54) N. Jayasuriya, S. Bosak, S.L. Regen, *J. Am. Chem. Soc.* **1990**, 112, 5844–5850.
- 55) V. Weissig, H.J. Mogel, M. Wahab, J. Lasch, *Proc. Intl. Symp. Control. Rel. Bioact. Mater.* **1998**, 25, 312.
- 56) V.V. Andrushchenko, H.J. Vogel, E.J. Prenner, *Biochim. Biophys. Acta, Biomembr.* **2007**, 1768, 2447–2458.

- 57) M.R. Mozafari, in *Liposomes: Methods and Protocols, Volume 1: Pharmaceutical Nanocarriers (Methods in Molecular Biology)* ed. V. Weissig, Humana Press, New-York, 2010, 2, 29–50.
- 58) S. Chatterjee, D.K. Banerjee, in *Liposome Methods and Protocols (Methods in Molecular Biology)* ed. S.C. Basu, M. Basu, Humana Press, New-York, **2002**, 1, 3–16.
- 59) S. Mallick, L.T. Thuy, S. Lee, J.I. Park, J.S. Choi, *Colloids Surf. B Biointerfaces* **2018**, 161, 356–364.
- 60) S.V. Boddapati, P. Tongcharoensirikul, R.N. Hanson, G.G. D'Souza, V.P. Torchilin, V. Weissig, *J. Liposome Res.* **2005**, 15, 49–58.

## All figure captions

**Figure 1** Chemical representation of the cationic bolaamphiphile dequalinium.

**Figure 2** Encapsulation efficiency of dequalinium in liposomes (eggPC/CH/DSPE-PEG<sub>2000</sub> 65/30/5) made in water or PBS after 24h of storage at 4°C (a). Liposomes were centrifuged (10 min; 10,000 g) and then ultrafiltrated to remove precipitated DQ prior to measurements.  $\zeta$ -potential variation of empty and DQ liposomes (10% of DQ) made in PBS (b) and water (c) immediately after preparation and after 24h of storage at 4°C. For these experiments, organic solutions of dequalinium and lipid mixture were dried to obtain a film that was then rehydrated and extruded to form small unilamellar vesicles. Values are mean of three independent experiments (mean  $\pm$  SD;  $n = 3$ ).

**Figure 3** Influence of DQ on  $\zeta$ -potential of after addition to pre-formed liposomes (eggPC/CH/DSPE-PEG<sub>2000</sub> 65/30/5) made in water (white circles) or PBS (black circles) (a). Influence of DSPE-PEG<sub>2000</sub> on  $\zeta$ -potential difference after addition of 10% DQ (molar ratio) to empty liposomes with different proportions of DSPE-PEG<sub>2000</sub>.  $\Delta\zeta_P = \zeta_P(\text{liposomes} + 10\% \text{ DQ}) - \zeta_P(\text{empty liposomes})$  (b). Association efficiency of 10% (molar ratio) DQ added to liposomes (eggPC/CH/DSPE-PEG<sub>2000</sub> 65/30/5) made in PBS (black) and in pure water (white) c). Values are mean of three independent experiments (mean  $\pm$  SD;  $n = 3$ ).

**Figure 4** DSC thermograms of fully hydrated (90% weight) DQ/DMPC mixtures in pure water (increasing ratios from bottom to top, the ratio was expressed in mol%) obtained at a rate of 2°C.min<sup>-1</sup> during heating. The inserts show enlargements of the pre-transition (a). Variations as a function of DQ proportion of onset ( $\blacktriangle$ ) and endset ( $\blacktriangledown$ ) temperatures (b) and enthalpies (c) of the pretransition (dotted line) and of the main transition (full line). Temperature uncertainties are obtained from the linear fit of temperatures (see experimental part 2.6) and enthalpy values are mean of at least three experiments (mean  $\pm$  SD;  $n \geq 3$ ).

**Figure 5** FF-TEM images of DMPC membranes rehydrated in pure water (a, b, c, d) or in PBS (e, f) containing 0% (a, e), 1% (b), 2.5% (c) and 5% (d, f) of DQ. Scale bar represents 1  $\mu\text{m}$ .



**Figure 6** SAXS and WAXS patterns of DMPC membranes in pure water containing different ratios of DQ (from bottom to top: 0, 2.5, 5 and 10 mol% of DQ) at 5°C (a), 20°C (b) and 40°C (c). For clarity, patterns are offset along the y-axis.

**Figure 7** SAXS patterns of DMPC membranes in PBS containing different ratios of DQ (from bottom to top: 0, 5 and 10 mol% of DQ) at 5°C (a), 20°C (b) and 40°C (c). For clarity, patterns are offset along the y-axis.

**Figure 8** Evolution of the bilayer thickness of DMPC membranes with or without DQ at 6°C or 32°C in pure water or in PBS. Bilayer thickness uncertainties are calculated from the fitting of SAXS profiles (see Figure S6).

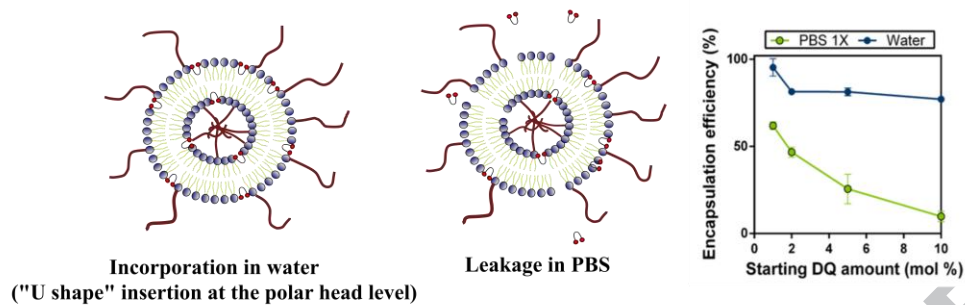
**Figure 9**  $^{31}\text{P}$ -NMR spectra of pure DMPC and DMPC containing between 1% and 10% of DQ in pure water at 6°C (a), 18°C (b) and 32°C (c). Panel d: chemical shift anisotropy (CSA) as a function of temperature of pure DMPC and DMPC containing 1% and 5% DQ.

**Figure 10** (a)  $^2\text{H}$ -NMR DePaked spectra of DMPC- $d_4$  membranes in pure water at pH 7 or in PBS recorded at 37°C with 0%, 1%, 3%, 5%, 10% of DQ. (b) Dequalinium concentration dependence of the quadrupolar splittings of the choline  $\alpha$  ( $\circ$ ,  $\square$ ) and  $\beta$  ( $\bullet$ ,  $\blacksquare$ ) methylene deuterons measured on the NMR spectra of panel (a), in pure water ( $\bullet$ ,  $\circ$ ) or PBS ( $\blacksquare$ ,  $\square$ ).

**Figure 11** Sketch of probable insertion of DQ in a lipid bilayer. DQ may induce membrane repulsion due to electrostatic interactions with negatively charged polar head groups of two adjacent bilayers in water leading to the formation of vesicles.

## Graphical abstract

### Influence of buffer for liposome formation in the presence of dequalinium chloride (DQ)



### Electrostatic interaction with lipid bilayers

